DOI: 10.21062/mft.2024.054 http://www.journalmt.com

Mechanical Properties and Compression Performance of 3D Printed HIPS Polymer Lattice Structure

Feng Jin (0009-0009-8369-256X)*, Wanqing Lu (0009-0009-7861-2262), Xu An (0009-0002-4059-0036), Haifeng Zhu (0009-0000-3670-3953), Jun Wang (0009-0002-9389-966X)
Southwest Construction Co., Ltd. of CSCEC 7th Division, Chongqing, 400043, China.
Corresponding author: fengjinchris@gmail.com

With the development of 3D technology, more and more materials are being used for manufacturing in many fields, such as factory manufacturing, workshop manufacturing, food packaging, even architectural design and civil engineering design. In particular, the mechanical properties of 3D printed HIPS polymer unit cell structures are worthy studying and analysing, providing more valuable references for future material development. This study focuses on the properties of HIPS polymer materials and the performance of HIPS polymer 3D printed lattice structures after compression test with Instron instrument. The experimental samples were divided into 4 groups, with4 different experimental variables for analysis and comparison. Finally, it was found that the HIPS polymer material has optimal compression resistance and relatively stable structure. In the future, it can be more applied in the fields of manufacturing, architectural design and civil engineering.

Keywords: 3D print, HIPS polymer, Compression test, Lattice structure, Stress and strain relationship

1 Introduction

Due to light weight and superior functionality of lattice structure, it is widely used in many fields of engineering [1]. The applications of ordinary polymer lattice structure include light-weight structures, energy absorption for collision and impact protection, and thermal transfer. Geometrical design, material and fabrication process will greatly affect the performance of lattice structure. Due to their respective process limitations, traditional manufacturing processes such as powder metallurgy and physical or chemical vapor deposition can achieve limited design freedom and porosity control. Incontrast, additive manufacturing (AM) provides geometric freedom and advanced features of the lattice structure to meet the requirements of applications. According to the ASTM standard, AM can be defined as the process of connecting materials to manufacture parts based on 3D model data, typically incremental rather than subtractive or forming manufacturing methods [2].

The state of equilibrium between external and internal forces of HIPS polymer lattice structure under load is usually considered as structural stability. The relative density of HIPS is 1.04-1.06, and the heat deformation temperature is 70-84℃, and the elongation of HIPS is about 35-60% [3]. Usually, the stronger the deformation resistance of the HIPS polymer lattice structure, and the better the structural stability. The mechanical properties of the lattice structure of the High Impact Polystyrene (HIPS) polymer manufactured by the additive manufacturing method (AM), especially the compression resistance, have a great influence on the future utilization and development of the HIPS polymer [3-4]. Therefore, it is of great value to study and explore the properties, mechanical properties, and compressive strength of the lattice structure of 3D printed HIPS polymers [4-5].

The main purpose is to learn and familiarize the crystal structure model of 3D printed HIPS polymer, and to make 4 different samples for experimental comparison. The Instron instrument in the laboratory was used to compress the 3D printed samples to record the complete deformation process and compression performance. The samples are subjected to mechanical analysis and chart interpretation by Instron software. The experimental results of the four test samples were analyzed and compared. Through this method, the compressive and mechanical properties of 3D printed HIPS polymer lattice structures are evaluated [6-8].

2 Methods and materials

2.1 3D printing process

Normally, 3D printing process includes design, file processing, production, finishing and socializing. Detailed description is as follows:

Design - Create the 3D files designed by Auto CAD or Solid Works, and then print from scratch. Sometimes, basic files can be obtained through digital scanning or downloading from network resources.

File processing- Prepare files for 3D printers by analyzing, uploading and rendering files using programs available locally installed or in cloud [5-6].

Production- Using different techniques based on the speed, accuracy, durability, quality of finished product and cost of materials.

Finishing-A variety of methods are used to finalize the parts to make them aesthetically pleasing and more durable.

Socializing-Part files, rendered images or photos can be shared on social media or on the free markets [7-8].

2.2 Method of 3D printing

There are many methods for 3D printing, mainly depending on different materials. The most common one is Fused Deposition Modeling (FDM) [2]. It uses a single nozzle head to extrude the melted material (usually resin or plastic) layer by layer onto the build platform based on 3D data provided to the printer. The FDM method is used to describe the familiar printer - Zortrax M300.

FDM is commonly used for modeling, prototyping and production, and it is also an additive manufacturing technology. "Additive" principle means placing materials in layers. The plastic or resin filament is usually unwound from a coil and supplies the material to an extrusion nozzle that can open or close the flow. The nozzle is heated so that the material can be melted as well [10]. It can be moved horizontally and vertically through a digital control mechanism and be directly controlled by a computer-aided manufacturing (CAM) software package. Since the material hardens immediately after extrusion from the nozzle, small beads of thermoplastic material can be extruded to create a model for the production layer. A stepper motor or a servo motor is usually used to move the extrusion head. Fig. 1 shows the details of 3D printer extruder [9, 11].

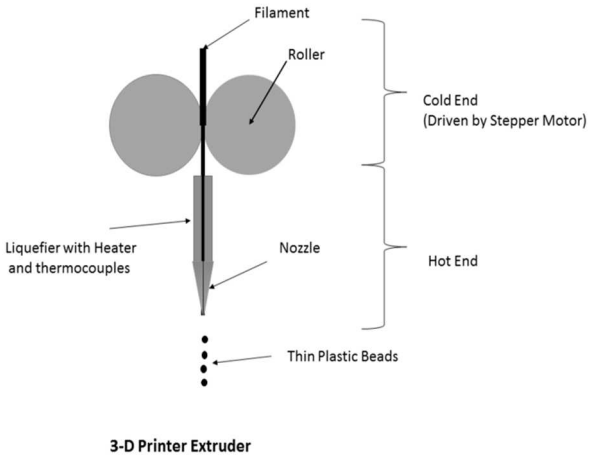

Fig. 1 *3D printer extruder*

The advantages of FDM are as follows:

- Low cost. The fused deposition modeling technology uses the laser instead of a liquefier with a low equipment cost; the utilization efficiency of the raw materials is high, and there is no pollution of poisonous gas or chemicals, greatly reducing the molding cost.
- The raw materials are provided in the form of reel wire and is easy to handle and quick to change, as shown in Fig. 2.
- A variety of materials can be selected, such as engineering plastics ABS, PC, PPS and medical ABS in different colors.
- The raw material has no chemical change during the molding process, and the warpage of the manufactured product is small.
- The FDM system is non-toxic and does not generate odor, dust, noise, or other pollutants. There is no need to build and maintain a dedicated venue suitable for office design.
- The material has excellent strength and toughness and can be assembled for functional testing [12-14].

Fig. 2 *Raw materials of HIPS for 3D printer*

2.3 Basic Mechanism of Experiments

2.3.1 The purpose of experiment

The compression properties of polymer materials are determined by testing their compressive strength, compressive modulus, and compressive strain.

2.3.2 The principle of experiment

In this experiment, a static compressive load is applied to the sample in the axial direction at

a specified experimental temperature, humidity, and acceleration to determine the mechanical properties of the HIPS polymer material [15].

Compression test is the most common type of mechanical test. Compression performance testing involves placing the sample between two pressure plates of a universal testing machine and applying a measurable size at a constant rate along the main axis of the sample end faces. The same opposite forces cause the sample to shorten in the axial direction and increase in the radial direction, resulting in compression deformation until the sample ruptures or deforms to a predetermined value, such as 25%. Directly reading the applied load from the testing machine, the compressive stress is defined as follows:

$$\sigma_i = \frac{P_i}{F_i} \quad (1)$$

Where:

σ_i…Compressive stress, MPa;

P_i…Compression load, N;

F_i …The original cross-sectional area of the sample, mm^2.

Compressive yield stress refers to the stress at the turning point (yield point) where the strain increases and the stress does not increase for the first time on the stress-strain curve, in MPa. Compressive strength refers to the maximum compressive stress experienced by a specimen during the compression test, in MPa. It is may not necessarily be the compressive stress experienced by the specimen at failure. Constant strain compressive stress refers to the compressive stress at a specified strain, that is, the stress value corresponding to the strain of 25%, in MPa. The change in sample height under compressive load is called compression deformation, and calculated as follows:

$$\Delta H_i = H_{0_i} - H_i \quad (2)$$

Where:

ΔH_i…Compression deformation of the specimen, mm;

H_{0_i}…Sample height, mm;

H_i…The sample height at any time during the compression process, mm.

The compression deformation of the sample divided by the original height of the sample is used as the compressive strain ε, and calculated as follows:

$$\varepsilon_i = \frac{\Delta H_i}{H_{0_i}} \quad (3)$$

Where:

ε_i…Sample compressive strain;

ΔH_i …Compression deformation of the sample, mm;

H_{0_i}…Sample height, mm;

H …The sample height at any time during the compression process, mm.

Compression modulus is the ratio of compressive stress to compressive strain in the linear range of the stress-strain curve, in MPa. The ratio of the stress difference between the two points on the stress-strain line to the corresponding strain is defined as follows:

$$E_{i,j} = \frac{\delta\sigma_{i,j}}{\delta\varepsilon_{i,j}} \quad (4)$$

Where:

E…The compressive modulus of the sample, unit MPa [10, 13, 16].

2.4 Experiments process mechanism

The preparatory process requires software design, file processing, and file rendering steps before formalizing the 3D printer manufacturing sample.

2.4.1 The 3D Part File Designed By AutoCAD

First, the body centered cubic (BCC) unit cell is designed by AutoCAD software, as shown in Fig. 3. The dimension of each cubic unit cell is 6×6×6 mm, and the diameter of the cylinder in the unit cell is 1.5 mm.

The sample models to be fabricated are then assembled from different number of unit cells in different directions. Four groups of HIPS polymer lattice structures are designed here.

The variable factor of the first group is with/without a top plate or bottom plate, which consists of 5 * 5 * 5 repeated body centered cubic (BCC) that labeled as lattices P1, P2, P3 and P4 (5 * 5 * 5 BCC unit cell samples) respectively (Fig. 4).

The variable test parameters of the second group are the number of BCC unit cells. They are also designed by AutoCAD software with 3 * 3 * 3, 4 * 4 * 4, 5 * 5 * 5, 6 * 6 * 6, 7 * 7 * 7, 8 * 8 * 8 repeated body centered cubic (BCC) that labeled as lattices N3, N4, N5, N6, N7, N8 respectively. All second group samples consist of a top plate and bottom plate at each end.

The lattice structures of the third BCC group will change the dimension of the unit cells and the diameter of the cylinder. Using AutoCAD software, the 5 * 5 * 5 BCC lattice samples are designed with a unit dimension of 4 mm and a diameter of 1 mm, a unit dimension of 6 mm and a diameter of 1.5, and a unit dimension of 8 mm and a diameter of 2 mm, respectively. The final set of variable factors is a different numbers of vertical unit cells named NV1 (5 * 5 * 3), NV2 (5 * 5 * 5) and NV3 (5 * 5 * 7).

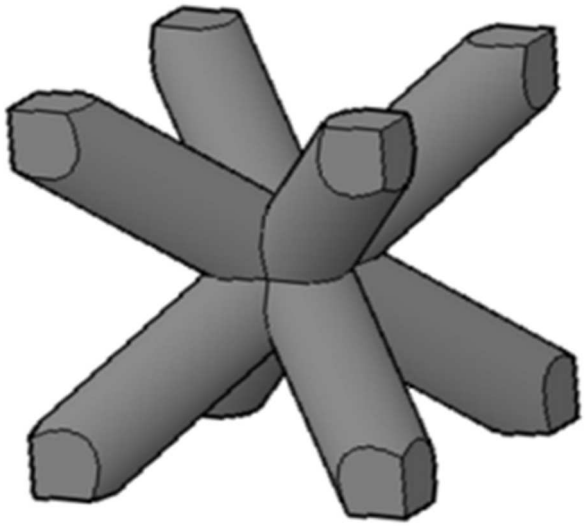

Fig. 3 *Body centered cubic (BCC) unit cell*

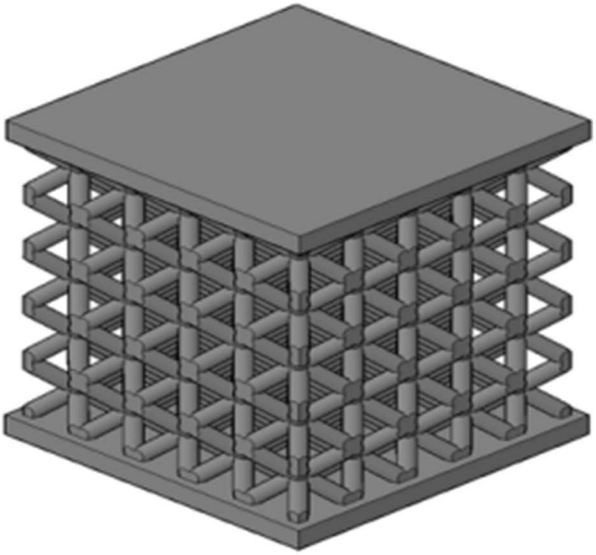

Fig. 4 *5*5*5 BCC unit cell*

2.4.2 Pre-processing software – Z-SUITE

After design, all group samples are saved in Stereo lithography (STL) file format. Ultimately, the files are imported into the pre-processing software, as shown in Fig. 5.

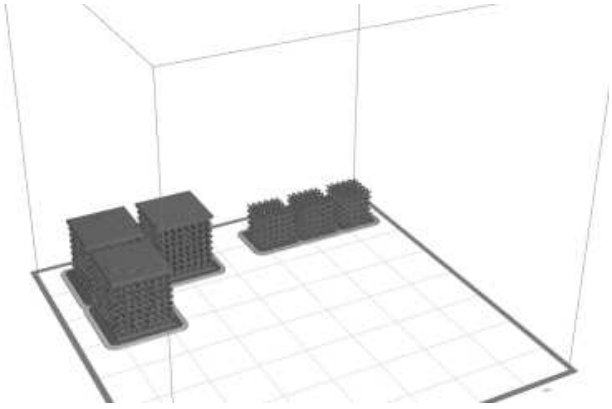

Fig. 5 *Preview of the HIPS polymer lattice structure in the Z-SUITE*

2.4.3 The Samples for Fabrication

Fig. 6 shows some of the HIPS polymer lattice structures being fabricated by the 3D printer. Fig. 7 shows the completed experimental samples.

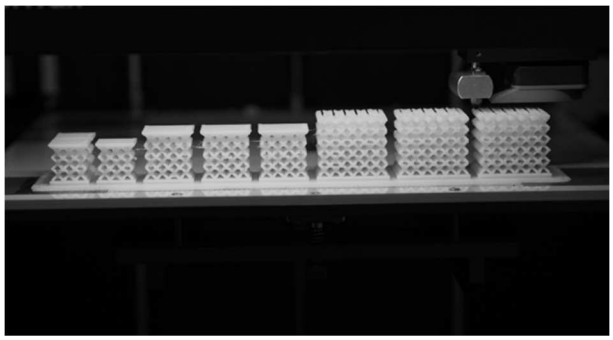

Fig. 6 *The printing process of 3*3*3, 4*4*4 and 6*6*6 BCC unit cell samples*

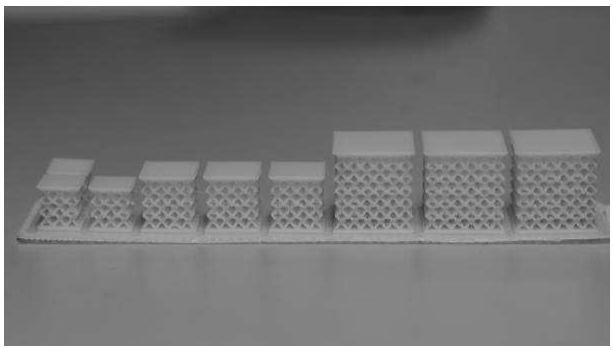

Fig. 7 *The printed samples*

2.5 Compressive behavior

Before the compression test, laboratory equipment must be equipped and checked. For the Instron compression test, two platens are required:

Top platen: Position the Check Nutuntil it becomes loose, align the Platen Clevis to the Clevis in the Load Cell, insert the Clevis Pin through the Clevis, attach the Retaining Clip, manually tighten the Check Nut counter-clockwise until it is touches the Load Cell, and use the provided Tommy Bar for assistance, but do not over tighten. Details are shown in Figure 8.

Bottom platen: first check if the compression Spring is placed inside the bottom Base Adapter, position the Check Nut until it becomes loose, align the Platen Clevis to the Clevis in the Base Adapter, pass the Clevis Pin through the Clevis and connect the Retaining Clip; finally, manually tighten the Check Nut clockwise until it is touches the Load Cell, and use the provided Tommy Bar for provide assistance, but do not over tighten. The installation diagram of bottom platen is shown in Figure 9.

After the installation steps are completed, the compression test could be started. The compression deformation and displacement change process of the sample can be recorded by the camera, as shown in Figure 10 [17]. A smart phone can be placed on the

side of the experimental platform, and its the video recording function can record the side view of the compression deformation and displacement change of the experimental samples, making the experimental data more perfect and accurate.

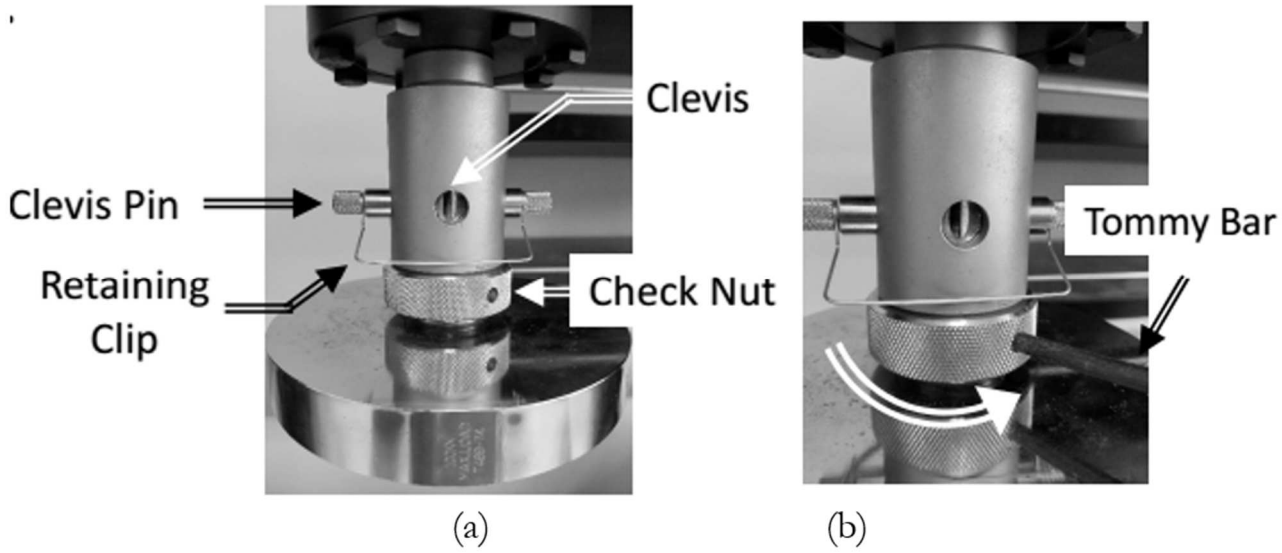

Fig. 8 *Installation diagram for top platen*

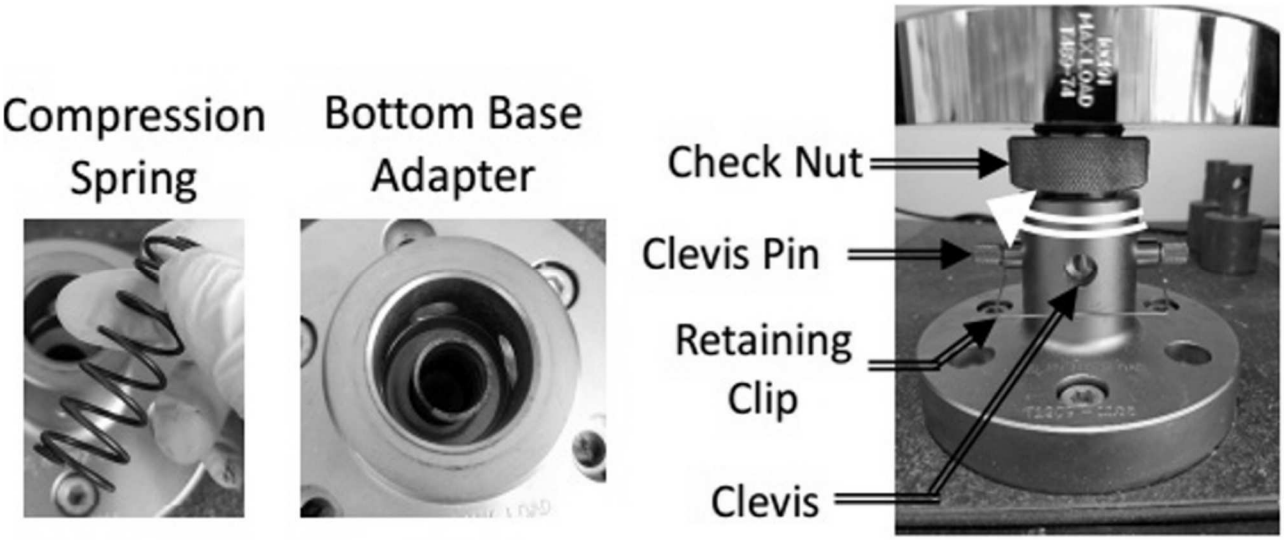

Fig. 9 *Installation diagram of bottom platen*

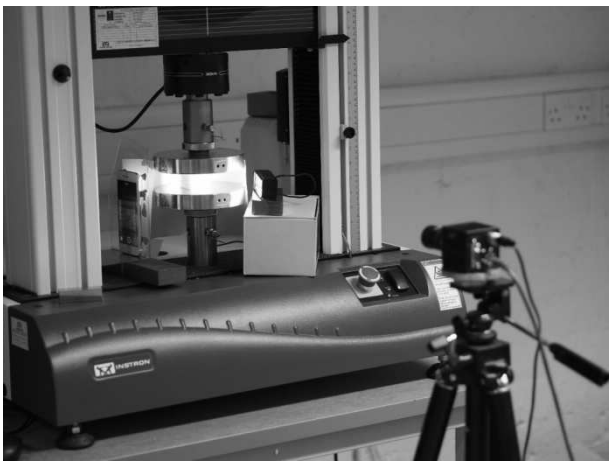

Fig. 10 *The placements of the experimental instruments*

Fig. 11 *Test rate setting from the Instron software*

In addition, for experimental samples with a numerical height of 30mm, a constant displacement rate of 0.03mm/s and a preload of 20N are applied. If the vertical height of the sample is 48mm, the constant displacement rate should be 0.048 mm/s, as shown in Figure 11 of the Instron software. After the compression tests, all tests data can be found in the computer.

Compression tests were conducted on all samples, and the relationship between force and displacement at each stage of the compression was recorded [18-19]. As shown in Fig. 12, it is the compression behavior of 5*5*5 sample 1.

Due to the fact that the direction of constructing samples during the printing process was from the bottom to the top of the graph, the order of folding layers seems to be independent of the direction of constructing samples.

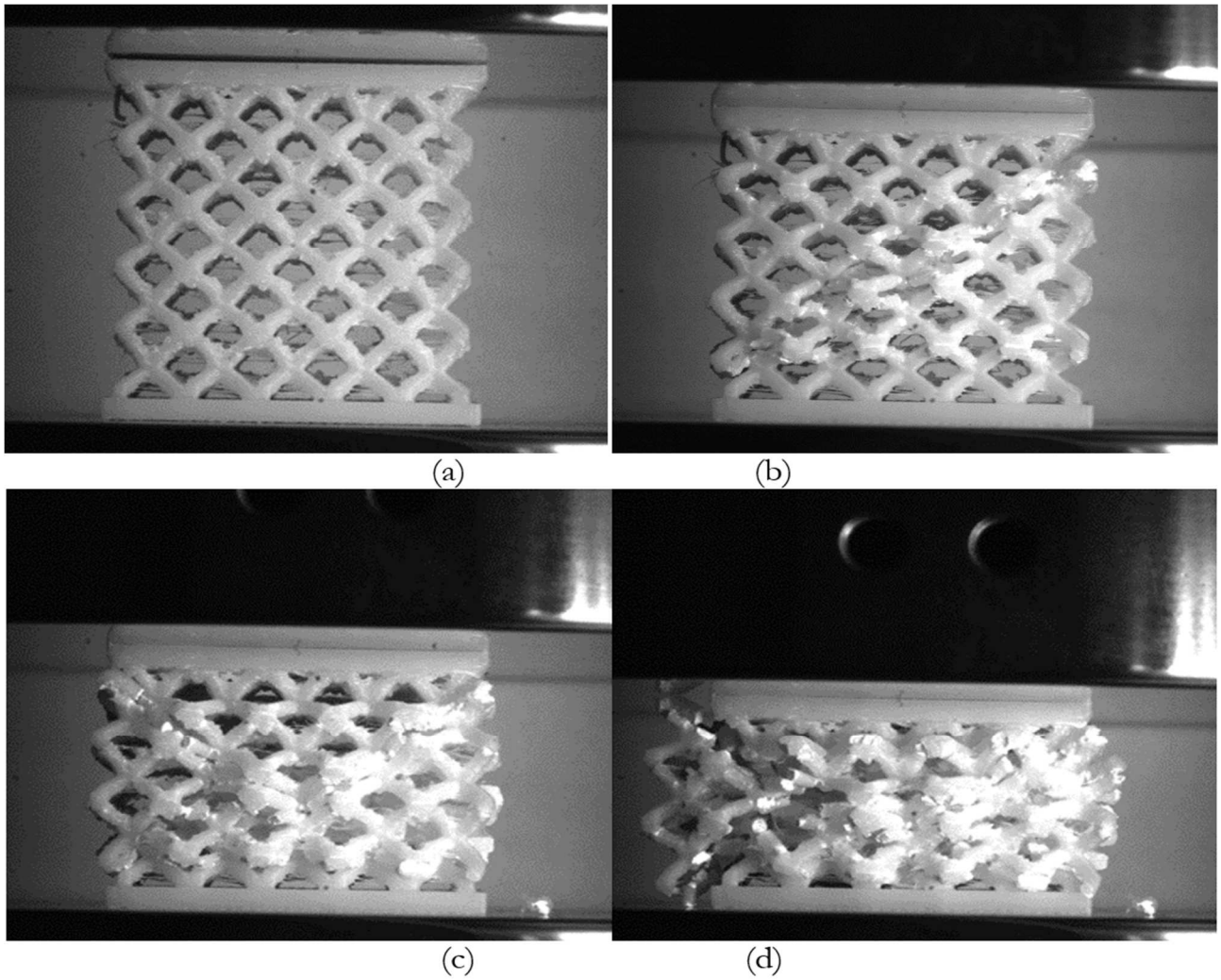

Fig. 12 *Compression behavior of5*5*5 sample 1*

During the compression test, a total of three sets of samples with different parameters or variables were compressed, and the force and displacement were recorded by using the software from the Instron laboratory instrument. Then, the stress-strain curve relationship for each test sample was calculated [20].

3 Results and Analysis

3.1 The force and displacement relationship of the 4 groups of samples

In the experimental result data of the 4 groups of compression tests, different positions of BCC unit cell plates, different number of BCC unit cells, different dimensions of strut BCC unit cells and different number of vertical BCC unit cells are shown in Fig. 13, Fig. 14, Fig. 15 and Fig. 16, respectively. Table 1, Table 2, Table 3 and Table 4 represent the basic test data under different groups of experimental performance respectively. Each group had three identical samples and conducted three compression tests. The deviation values of the obtained displacement data are controlled within 0.1mm, and the average value is finally calculated to make the test sample data more scientific and of reference value. All figures are related with the force and displacement relationship. The unit cells of force and displacement are N and mm respectively.

Tab. 1 *Measured physical and geometrical properties of the lattice blocks after the compression tests at different plate positions*

Type of Sample	Subsample Number	Designed strut diameter (mm)	Length in horizontal (x direction)	Length in horizontal (y direction)	Length in vertical
P1	NO.1	1.57	30.26	30.21	30.07
	NO.2	1.56	30.04	30.03	30.22
	NO.3	1.51	30.15	30.17	30.39
P2	NO.1	1.52	30.07	30.05	30.05
	NO.2	1.53	30.11	30.15	30.06
	NO.3	1.59	30.18	30.37	30.09
P3	NO.1	1.56	30.20	30.24	29.45
	NO.2	1.65	30.15	30.07	29.50
	NO.3	1.65	30.10	30.14	29.50

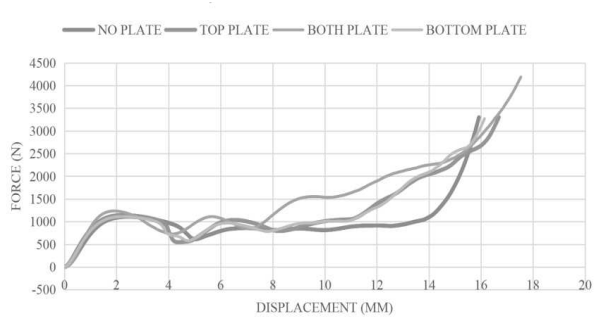

Fig. 13 *Force displacement relationship of different positions of BCC unit cells plate*

Table 1 shows the different numbers of unit cells measured for the physical and geometrical properties of lattice blocks after compression tests. As shown in Fig. 13, when the three samples (5*5*5 BCC with top plate, bottom plate, no plates and both plates) reach the yield strength, the maximum forces are similar with 1.1446 kN, 1.1112 kN, 1.107 kN and 1.234 kN, respectively. However, it is clear that the curves of the top plate and the bottom plate are similar in Fig. 13, and the trajectories of the force and displacement diagrams are almost identical. The plate position of HIPS-BCC unit cell lattice is the top or bottom plates, which has little effect on the mechanical properties of the structure. However, the detailed results will be explained in the stress-strain diagram in the next section. For the two curves with and without plates, the values of their forces are similar when structural buckling is reached. However, in the densification phase, the force of the mesh structure with the bolt plate is significantly greater than the latter.

Tab. 2 *Different numbers of unit cells measured for the physical and geometrical properties of the lattice blocks after compression tests*

Type of Sample	Subsample Number	Designed strut diameter (mm)	Length in horizontal (x direction)	Length in horizontal (y direction)	Length in vertical
N3	NO.1	1.52	18.23	18.28	18.01
	NO.2	1.52	18.20	18.21	18.06
	NO.3	1.54	18.08	18.10	18.03
N4	NO.1	1.53	24.21	24.17	24.02
	NO.2	1.51	24.22	24.13	24.02
	NO.3	1.54	24.28	24.18	24.01
N5	NO.1	1.53	30.25	30.15	30.21
	NO.2	1.54	30.34	30.25	30.94
	NO.3	1.53	30.31	30.14	30.21
N6	NO.1	1.52	36.00	36.08	36.13
	NO.2	1.51	36.09	36.10	36.02
	NO.3	1.52	36.04	36.05	36.10
N7	NO.1	1.52	42.67	42.19	42.25
	NO.2	1.52	42.32	42.26	42.16
	NO.3	1.54	42.28	42.41	42.06
N8	NO.1	1.55	48.09	48.02	47.94
	NO.2	1.52	48.02	48.26	47.93
	NO.3	1.54	48.31	48.37	47.81

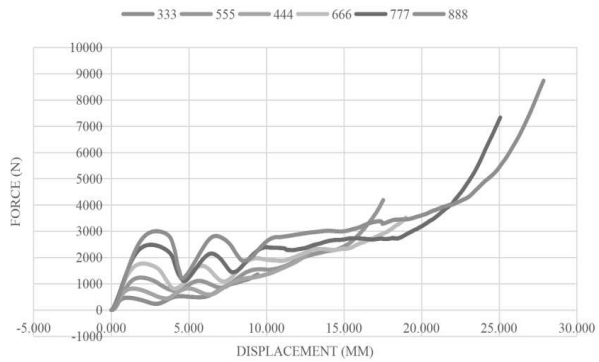

Fig. 14 *Force displacement relationship of different numbers of BCC unit cells*

Table 2 shows the different numbers of unit cells measured for the physical and geometrical properties of lattice blocks after compression tests. In theory, under the same material conditions, the more the unit cell, the more stable the structure and the greater the pressure it can withstand. The experimental results are also consistent with expectations. For instance, as shown in Fig. 14, the first peak of the force is about0.4683 KN in 3*3*3BCC curve, while the number are 0.8175 kN of 4*4*4 BCC unit cell, 1.234 kN of 5*5*5 BCC unit cell and 1.769 kN of 6*6*6 BCC samples, respectively. In addition, the first force peak of 7*7*7 BCC and 8*8*8 BCC samples are 2.483 kN and 2.999 kN, respectively. More specifically, due to the increase of body centered cubic (BCC) unit cells, the force of 4*4*4 sample reaching the yield strength is 74.57% higher than the first force peak of 3*3*3 sample. Similarly, the same value of 5*5*5 BCC unit cell is 50.95%, more than 4*4*4 BCC, and the peak of the first force of 6*6*6 BCC is 43.35%,higher than 5*5*5 BCC. The values for 7*7*7 sample and 8*8*8 sample are 40.36% and 20.78%, respectively. Therefore, for some reasons, the samples can bear greater compressive pressure as the BCC unit cells increases, while the rate of growth decreases. On the contrary, the growth rate is faster when the number of BCC unit cells is small. On the other hand, as shown in Fig. 14, during the densification stage, under the same compression test conditions, the more number of the BCC unit cells, the more force the structure can bear. A detailed analysis will be explained in the stress-strain relationship diagram in the next section [21].

Tab. 3 *Different dimensions strut of unit cells measured for the physical and geometrical properties of lattice blocks after compression tests*

Type of Sample	Subsample Number	Designed strut diameter (mm)	Length in horizontal (x direction)	Length in horizontal (y direction)	Length in vertical
D=1 mm	NO.1	1.21	20..63	20.23	20.21
	NO.2	1.23	20.19	20.20	20.08
	NO.3	1.19	20.23	20.04	20.08
D=1.5 mm	NO.1	1.53	30.25	30.15	30.21
	NO.2	1.54	30.34	30.25	30.94
	NO.3	1.52	30.31	30.14	30.21
D=2 mm	NO.1	2.07	40.12	40.03	40.15
	NO.2	2.13	40.27	40.25	40.10
	NO.3	2.08	40.32	40.27	40.24

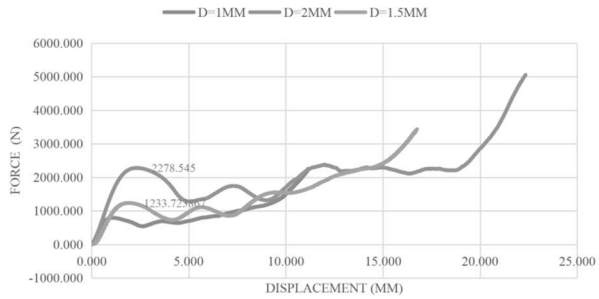

Fig. 15 *Force displacement relationship of different dimensions of strut BCC unit cells*

Table 3 shows the different dimensions strut of unit cells measured for the physical and geometrical properties of lattice blocks after compression tests. Fig. 15 shows the force and displacement of different dimensions of strut BCC unit cells. Taking 5*5*5 BCC unit cell as an example, its D=1.5 mm corresponds to a design unit side length of 6 mm. When the pressure begins to compress the sample, its displacement also begins to increase. It starts from a linear elastic phase in Fig. 15. After the following nonlinear phase, its force reaches the first peak. At this point, the structure reaches the yield strength (the stress and strain relationship diagram will be detailed in following section), which is about 1.234 kN. For comparison, in the force and displacement diagram of samples with a diameter of 1 mm and a diameter of 2 mm, the two first peaks of force are about 2.27 kN and 0.792 kN, respectively. It is clear that under the same conditions, the larger the design diameter, and the greater

the force the structure can bear. Similarly, the 3D printed samples of D=2 mm can withstand more compressive pressure during the densification or compaction phase [21-23].

Tab. 4 *Different numbers of vertical unit cells measured for the physical and geometrical properties of lattice blocks after compression tests*

Type of Sample	Subsample Number	Designed strut diameter (mm)	Length in horizontal (x direction)	Length in horizontal (y direction)	Length in vertical
NV1	NO.1	1.50	30.21	30.24	18.08
	NO.2	1.52	30.34	30.26	18.01
	NO.3	1.56	30.15	30.08	18.07
NV2	NO.1	1.53	30.25	30.15	30.21
	NO.2	1.54	30.34	30.25	30.94
	NO.3	1.52	30.31	30.14	30.21
NV3	NO.1	1.52	30.14	30.12	42.17
	NO.2	1.51	30.09	30.12	42.01
	NO.3	1.57	30.11	30.02	42.01

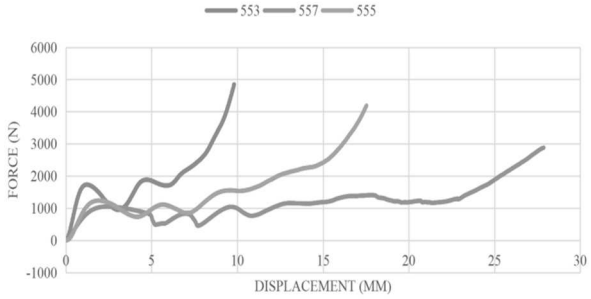

Fig. 16 *Force displacement relationship of different numbers of vertical BCC unit cells*

Table 4 shows the different numbers of vertical unit cells measured for the physical and geometrical properties of lattice blocks after compression tests. As shown in Fig. 16, the force decreases as the vertical unit cells increase when the yield strength occurs. The force peak of 5*5*3 BCC curve is about 1.731 kN, and 1.234 kN and 1.050 kN for 5*5*5 BCC and 5*5*7 BCC respectively. More specifically, the value of 5*5*3 BCC is 40.28%, higher than that of 5*5*5 BCC, while the first force peak data of 5*5*7 BCC is 17.5%.Therefore, as the vertical unit cells decrease, the growth rate of the first force peak in force displacement curve increases. As a result, under the same conditions, the shorter the grid structure and the more stable the mechanical behavior.

3.2 The Strain-Stress Relationship Diagrams of the 4 Groups

According to the force displacement curve of each test sample and the calculation principles in Section 2, the stress and strain curve of each group of samples are shown as Fig. 17, Fig. 18, Fig. 19 and Fig. 21, respectively. All the testing and calculation data are shown in Table 5, Table 6, Table 7 and Table 8.

In case of the top and bottom plates, their stress-strain curves are almost the same within a certain experimental error. As shown in Table 5, their yield strain and compressive modulus are 0.0750 MPa, 0.0760 MPa and 30.7982 MPa, 32.3431 MPa, respectively. During the compression experiment, only one HIPS lattice BCC unit cell structure plate (whether on top or bottom) has the same experimental results. This will not have a great impact on the mechanical properties and stability of the lattice structure. On the other hand, the stress-strain curves of the four different samples are relatively selected. From Table 5, it can be seen that the sample with a bolt plate has the maximum yield strain of 39.1310 MPa, while the test strain without a plate has the minimum yield strain of 29.4299 MPa. In Fig.17, after the failure stage, the stress-strain curves have many small fluctuations due to the randomness of each sample and certain experimental errors. It is evident that during the densification/ follow-up elastic stage, samples with two plates can withstand greater compressive stress when the same nominal strain is generated. The followed is a HIPS cell structure with one plate, and then is an experimental sample without a plate. The periodic plateau stresses in Fig.17 have a slight undulation, and the sample with two plates has the maximum value (1.420 MPa), followed by only one plate (1.267 MPa and 1.256MPa), and then no plate (1.228 MPa).

The plate still has a significant impact on the grid structure within a certain range, as it binds the unit cells in contact. During the compression test, the plate maintains contact witall unit cells to prevent premature separation from the HIPS lattice structure. On the contrary, compared with other samples, samples without plate protection move freely during the compression test, losing plate binding. It results in more pronounced structural buckling and reducing

plateau stress values in the densification follow-up elastic stage.

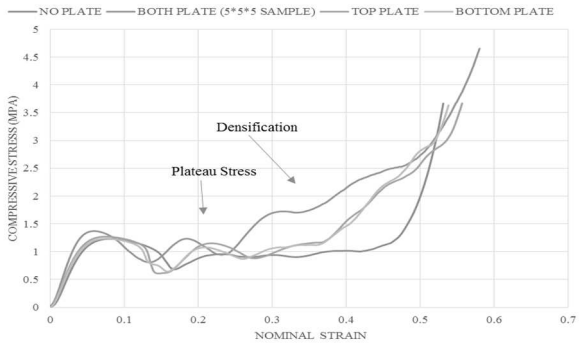

Fig. 17 *Effects of boundary conditions (Group 1)*

When the compression test parameters are different number of unit cells, a large number of test samples with different specifications should be used to reduce experimental errors. Fig. 18 shows the compression behaviors of different number of unit cells in the HIPS lattice structures, with sample sequence numbers N3-N8. Like the previous stress strain, the curve in Fig. 18 also has four stages: elastic stage, nonlinear stage, damage stage and densification/ follow-up elastic stage. However, in the initial elastic deformation region, the curve trajectories of all test samples are almost the same, that is, their slopes are not similar, and their compressive modulus are ε_{3niti} =42.7316 MPa, $\varepsilon_{442.7}$ =40.5374 MPa, $\varepsilon_{540.5}$ =39.1310 MPa, $\varepsilon_{6=39.}$ =38.9316 MPa, $\varepsilon_{738.9}$ =38.6233 MPa and $\varepsilon_{838.6}$ =37.3613 MPa, respectively, as shown in Table 6. More specifically, as the number of unit cells increases, the compression modulus of the HIPS polymer lattice structure decreases, that is, the structural compressibility sequentially increases. This may be that when the number of BCC unit cells is small, the influence of structure with top and bottom plates is greater, and some crystal cells are more constrained to peel off from the structure, resulting in a more stable and better compression resistance. A larger number of BCC unit cells, such as 8*8*8 samples, is much larger than the volume of 3*3*3 samples. The top and bottom plates have less influence on the stability of the structure. During the compression test, the internal structure of the 8*8*8 samples is more easily destroyed, and the entire destruction process is easier to record.

Tab. 5 *All relevant data from the compression test of Group 1*

Type of samples	Compressive modulus-E (MPa)	Peak strength(MPa)	Yield strain	Plateau stress (MPa)
BOTTOM PLATE	30.7982	1.2352	0.0750	1.256
NO PLATE	29.4299	1.2304	0.0810	1.228
TOP PLATE	32.3431	1.2715	0.0760	1.267
BOTH PLATES	39.1310	1.3718	0.0589	1.420

For the peak strength of the test samples from N3 to N8, the value of 3*3*3 BCC unit cell is the maximum with 1.4452 MPa. Then the peak strength of 4*4*4 BCC unit cell and 5*5*5 unit cell are 1.4165 MPa and 1.3718 MPa, respectively, until the number of 8*8*8 BCC unit cell (1.3015) is the smallest. Therefore, as the number of unit cells increases, the peak strength of each set of experimental samples will decrease under the given experimental error conditions. As the increase in compression modulus, the compression performance of the test sample is better. Due to the small dimension of 3*3*3 samples, the top and bottom plates can better limit and constrain the unit cells that are in connected with them. Naturally, the 3*3*3 BCC unit cell lattice structure has better stability to a certain extent.

At the same time, as the number of unit cells increases, the decrease of peak strength is greatly reduced. Theoretically, under the same conditions, when the number of unit cells increases to a certain extent, the peak strength of all test samples will approach a stable value. However, due to uncertainties such as experimental conditions and experimental time, the number of unit cells could not be increased on the basis of 8*8*8 BCC unit cell samples.

In addition, the plateau stress also shows a natural decreasing trend, as shown in Table 6.

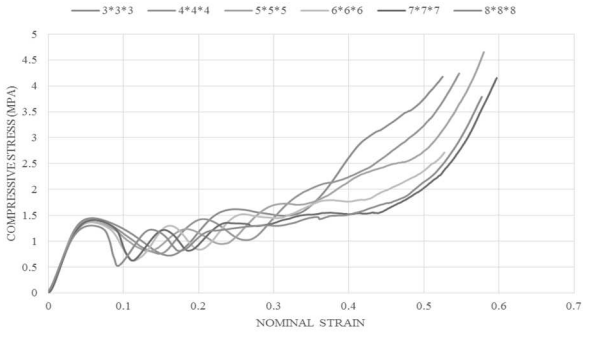

Fig. 18 *Effects of the number of unit cell (Group 2)*

Tab. 6 *All relevant data from the compression test of Group 2*

Type of samples	Compressive modulus-E (MPa)	Peak strength(MPa)	Yield strain	Plateau stress (MPa)
3*3*3	42.7316	1.4452	0.0575	1.711
4*4*4	40.5374	1.4165	0.0580	1.563
5*5*5	39.1310	1.3718	0.0589	1.420
6*6*6	38.9316	1.3647	0.0565	1.375
7*7*7	38.6233	1.4075	0.0605	1.352
8*8*8	37.3613	1.3015	0.0577	1.311

Tab. 7 *All relevant data from compression test of Group 3*

Type of samples	Compressive modulus-E (MPa)	Peak strength(MPa)	Yield strain	Plateau stress (MPa)
D=1 mm	63.6152	1.9818	0.0555	1.965
D=1.5 mm	39.1310	1.3718	0.0589	1.420
D=2 mm	40.9036	1.4242	0.0585	0.935

Fig. 19 shows the compression stress and nominal strain relationship plots of compression tests at different dimensions of strut unit cells. In this set of experiments, the structure of the 5*5*5 BCC unit cell is used, but the design value of the dimension of each strut unit cell is different, such as D (the dimension of unit cells)=1 mm; D= 1.5 mm and D=2 mm. Hereinafter referred to as D1, D1.5 and D2.

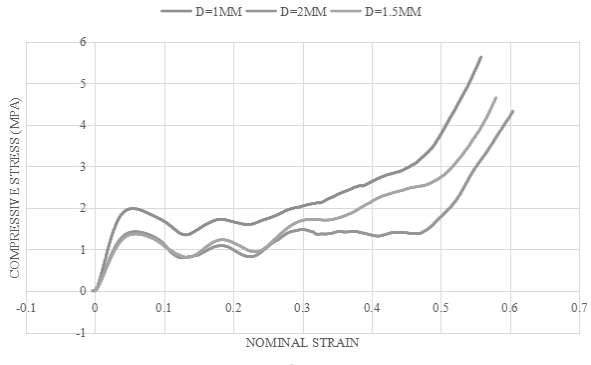

Fig. 19 *Effects of different dimensions of strut unit cells (Group 3)*

As shown in Fig. 20, the volume of the HIPS polymer lattice structure sample of D=2 mm (hereinafter referred to as D2) is much bigger than the same structure of D=1 mm (hereinafter referred to as D1). More specifically, after the compression test, the structural damage of the D2 sample is more pronounced, and some of the unit cells are stripped together and peeled off from the side of the sample. Local unit cells will be scattered and even ruptured into small struts. In the stress-strain curve of D2 sample in Fig. 19, the curve trend of its elastic phase and nonlinear phase is similar to D1.5. Their peak strengths are 1.4242 MPa and 1.3718 MPa, respectively. Their elastic moduli are 40.9036 MPa and 39.1310 MPa, respectively. These values are almost equal, but the values of D2 are slightly larger. However, after the damage phase, especially in the densification/follow-up elastic phase, the compression stress value of D1.5 is greater than that of D2 under the same nominal strain condition. From Table 7, it can be concluded that the plateau stress of D1.5 is 1.420. MPa, but the plateau stress of D2 is 0.935MPa. This may be due to the excessive volume of D2.The internal structure of the sample is more easily deformed outwards and extruded by the experimental instrument during the compression test, resulting in loose internal structure. In the process of experimental data collection, the stress in the failure stage should gently change to gradually rise and enter the compact stage.

In contrast, as shown in Fig. 19, the compressive modulus and peak strength of D1 are much larger than D1.5 and D2, which are 63.6152 Mpa and 1.9818 MPa, respectively. The nonlinear strain values when they are flexed aresimila, as shown in Table 7. Theoretically, the stress-strain curves of D1 and D1.5, D2 should be similar, and their compressive modulus and peak strength should be similar too. The reason for this difference may be experimental errors, or more precisely, inaccuracies during 3D printing process result in the actual dimension strut of D1 being greater than the design value. After experimental measurement, the actual dimension strut values of the three D1 samples are 1.21 mm, 1.23 mm and 1.19 mm, respectively, greater than the original design value (1.00mm). Therefore, the number of plateau stress of D1 is also1.965 MPa, greater than others.

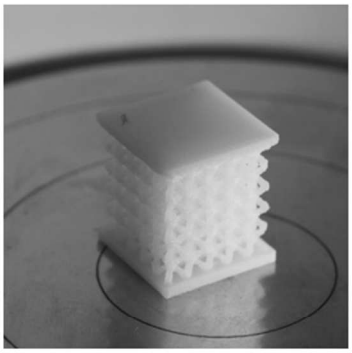

(a) 3D printed sample (D=1 mm)

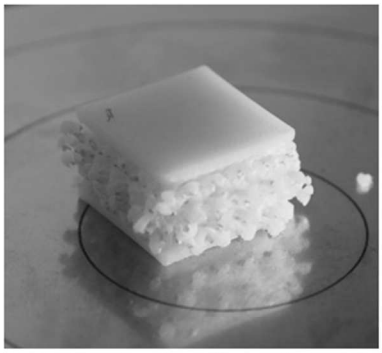

(b) 3D printed sample (D=1 mm)after compression test

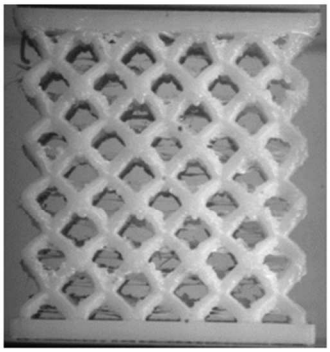

(c) 3D printed sample (D=1.5 mm)

(d) 3D printed sample (D=1.5 mm) after compression test

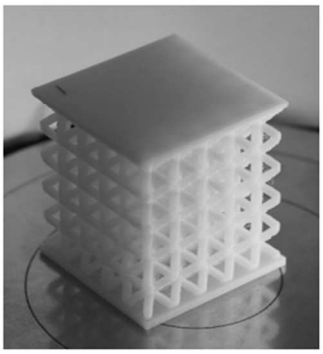

(e) 3D printed sample (D=2 mm)

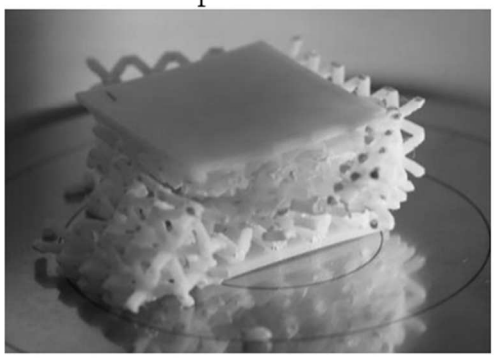

(f) 3D printed sample (D=2 mm) after compression test

Fig. 20 *The 3rd group samples*

As shown in Fig. 21 and Table 8, it can be found that the compressive moduli of NV1, NV2 and NV3 are 41.6423 MPa, 39.1310 MPa and 34.7876 MPa, respectively. As the numerical height increases, the compressive strength decreases. Similarly, the peak strength values of NV1, NV2 and NV3 also gradually decrease with 1.9230 MPa, 1.3718 MPa and 1.1667 MPa, respectively. However, for the stress-strain curve of NV3, due to 7 BCC unit cells in the vertical direction, the center of gravity of its structure is high. During the compression process, the internal influence of the plates on the overall structure is small. When the compression failure begins, the entire NV3 sample is surrounded. The unit cells structure begins to decline. The corresponding stress-strain curve also begins to change, shown as A and B phase in Fig. 21. Compared with the stable fluctuations of the curves NV1 and NV2, NV3 begins to decrease rapidly after reaching the yield strength, and then the fluctuation of the stress-strain curve is also significant.

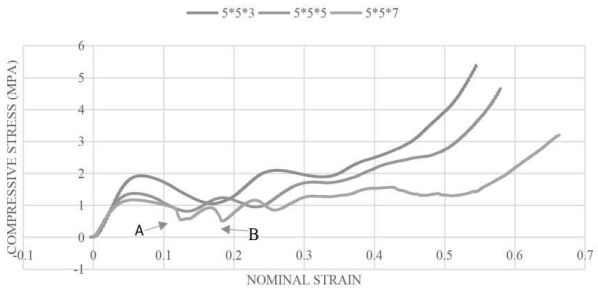

Fig. 21 *Effects of different numbers of vertical BCC unit cells (Group 4)*

Tab. 8 *All relevant data from the compression test of Group 4*

Type of samples	Compressive modulus-E (MPa)	Peak strength(MPa)	Yield strain	Plateau stress (MPa)
5*5*3	41.6423	1.9230	0.0685	2.086
5*5*5	39.1310	1.3718	0.0589	1.420
5*5*7	34.7876	1.1667	0.0575	1.203

4 Conclusions

The FDM method of 3D printer is used to fabricate the lattice structures of different cubic units. During the experiment, the structural design parameters were divided into 4 groups. Each group was compared to study the deformation behavior and compression performance of the HIPS polymer lattice structure. The main findings are as follows:

In terms of the effect of the plate on the HIPS polymer lattice structure, under the same design specifications, the structures without plates are more compressible than those with plates. In other words, their compression resistances are worse and more susceptible to damage. Energy absorption is also less for those without plates. Due to the binding effect of the plate on the structure, the structural stability of the HIPS polymer lattice structure can be improved to a certain extent. In terms of different number of unit cells, the more they are designed, and the better the mechanical properties of the 3D printed HIPS polymer lattice structure. On the contrary, the smaller number of unit cells in a certain size range, the more stable the lattice structure, and better compression resistance. On the other hand, when the design number of unit cells increases to a certain number, the peak strength of the crystal structure will approach a stable value. However, this accurate value cannot be obtained due to the limitation of experimental conditions.

For different dimensions of strut unit cells, due to the printing problem (printing accuracy needs to be improved) of the 3D printer, the actual sample may be larger than the strut dimension of the designed sample, and the experimental results will be greatly affected. On the other hand, considering different dimensions of struts, relative density of the samples needs to be considered, and more experiments are needed.

In terms of different numbers of vertical unit cells, as the number increases, the HIPS polymer lattice structure has a weaker stability and better compressibility, as well as weaker mechanical properties. The shorter in vertical direction, the more stable of HIPS polymer lattice structure, and the better compression resistance within a certain number of vertical unit cells.

In general, the HIPS polymer lattice structure has optimal stiffness and elasticity, and the structure is relatively stable. Within a certain range, it can absorb the energy released by compression. In the future, it can be more applied in the fields of manufacturing, architectural design and civil engineering in the future.

For future consideration, due to limitations of experimental sites and conditions, this study does not provide an in-depth discussion of some critical values of the HIPS polymer lattice structure in compression test. For example, as the number of unit cells increases, the peak strength of the sample approaches a stable value. At the same time, if the instrument can observe the microscopic image of the fracture surface of the test sample, more data can be provided to analyze and prove their structural stability and mechanical properties. The results can be applied to the prediction of stress-strain trend in the study of 3D printed HIPS polymer lattice structure, and can also be used as a reference for strength prediction, structural design and modeling design in the fields of manufacturing, architectural design and civil engineering. At the same time, this study provides a specific reference for future in-depth experimental exploration and has fundamental and far-reaching research significance.

Acknowledgement

First of all, I would like to express my heartfelt thanks and sincere respect to Professor Li Peifeng. My supervisor gave me tremendous help from beginning to end in the process of research direction, data collection, thesis topic selection, research work development, and finalization of the thesis. In addition, I would also like to thank the units that provided financial support for this research, and the company for its trust and support, which gave me the opportunity to use my talents and abilities here and contribute to the development and growth of the company.

References

[1] PAGAC, M., HAJNYS, J., MA, Q. P., JANCAR, L., JANSA, J., STEFEK, P., & MESICEK, J. (2021). A Review of Vat Photopolymerization Technology: Materials, Applications, Challenges, and Future Trends of

3D Printing. *Polymers*, Vol. 13, No.4, pp. 598. https://doi.org/10.3390/polym13040598

[2] KRISTIAWAN, R. B., IMADUDDIN, F., ARIAWAN, D., UBAIDILLAH, & ARIFIN, Z. (2021). A review on the fused deposition modeling (FDM) 3D printing: Filament processing, materials, and printing parameters. *Open Engineering*, Vol. 11, No. 1, pp. 639-649. https://doi.org/10.1515/eng-2021-0063

[3] BERCZELI, M., & WELTSCH, Z. (2021). Enhanced Wetting and Adhesive Properties by Atmospheric Pressure Plasma Surface Treatment Methods and Investigation Processes on the Influencing Parameters on HIPS Polymer. *Polymers*, Vol. 13, pp. 901. https://doi.org/10.3390/polym13060901

[4] SIGNORET, C., EDO, M., LAFON, D., CARO-BRETELLE, A. S., LOPEZ-CUESTA, J. M., IENNY, P., & PERRIN, D. (2020). Degradation of Styrenic Plastics During Recycling: Impact of Reprocessing Photodegraded Material on Aspect and Mechanical Properties. *Journal of Polymers and the Environment*, Vol. 28, pp. 2055-2077. https://doi.org/10.1007/s10924-020-01741-8

[5] ZHOU, L. Y., FU, J., & HE, Y. (2020).A Review of 3D Printing Technologies for Soft Polymer Materials. *Advanced Functional Materials*, Vol. 30, No. 28, pp. 2000187. https://doi.org/10.1002/adfm.202000187

[6] GOH, G. D., SING, S. L., & YEONG, W. Y. (2021). A review on machine learning in 3D printing: applications, potential, and challenges. *Artificial Intelligence Review*, Vol. 54, pp. 63-94. https://doi.org/10.1007/s10462-020-09876-9

[7] WICKRAMASINGHE, S., DO, T., & TRAN, P. (2020). FDM-Based 3D Printing of Polymer and Associated Composite: A Review on Mechanical Properties, *Defects and Treatments. Polymers*, Vol. 12, No. 7, pp. 1529. https://doi.org/10.3390/polym12071529

[8] YANG, C., KIM, Y., RYU, S., & GU, G. X. (2020). Prediction of composite microstructure stress-strain curves using convolutional neural networks. *Materials & Design*, Vol. 189, pp. 108509. https://doi.org/10.1016/j.matdes.2020.108509

[9] RASHID, M. M., PITTIE, T., CHAKRABORTY, S., & KRISHNAN, N. A. (2022). Learning the stress-strain fields in digital composites using Fourier neural operator. *Iscience*, Vol. 25, pp. 105452. https://doi.org/10.1016/j.isci.2022.105452

[10] ZAITSEV, V. Y., MATVEYEV, A. L., MATVEEV, L. A., SOVETSKY, A. A., HEPBURN, M. S., MOWLA, A., & KENNEDY, B. F. (2020). Strain and elasticity imaging in compression optical coherence elastography: The two-decade perspective and recent advances. *Journal of Biophotonics*, Vol. 14, No. 2, pp. e202000257. https://doi.org/10.1002/jbio.202000257

[11] ALAM, F., ELSHERIF, M., ALQATTAN, B., ALI, M., AHMED, I. M. G., SALIH, A., BUTT, H. (2020). Prospects for Additive Manufacturing in Contact Lens Devices. *Advanced Engineering Materials*, Vol. 23, No. 1, pp. 2000941. https://doi.org/10.1002/adem.202000941

[12] ZHOU, T., ZHU, J. B., JU, Y., & XIE, H. P. (2019).Volumetric fracturing behavior of 3D printed artificial rocks containing single and double 3D internal flaws under static uniaxial compression. *Engineering Fracture Mechanics*, Vol. 205, pp. 190-204. https://doi.org/10.1016/j.engfracmech.2018.11.030

[13] YE, G., BI, H., & HU, Y. (2020). Compression behaviors of 3D printed pyramidal lattice truss composite structures. *Composite Structures*, Vol. 233, pp. 111706. https://doi.org/10.1016/j.compstruct.2019.111706

[14] PARK, J. H., & PARK, K. (2020). Compressive behavior of soft lattice structures and their application to functional compliance control. *Additive Manufacturing*, Vol. 33, pp. 101148. https://doi.org/10.1016/j.addma.2020.101148

[15] MATUŠ, M., BECHNÝ, V., JOCH, R., DRBÚL, M., HOLUBJÁK, J., CZÁN, A., et al. (2023). Geometric Accuracy of Components Manufactured by SLS Technology Regarding the Orientation of the Model during 3D Printing. *Manufacturing Technology*, Vol. 23, No. 2, pp. 233-240. https://doi.org/10.21062/mft.2023.027

[16] AMANI, Y., DANCETTE, S., DELROISSE, P., SIMAR, A., & MAIRE, E. (2018). Compression behavior of lattice structures produced by selective laser melting: X-ray tomography based experimental and finite element approaches. *Acta Materialia*, Vol. 159, pp. 395-407. https://doi.org/10.1016/j.actamat.2018.08.030

[17] CRUPI, V., KARA, E., EPASTO, G., GUGLIELMINO, E., & AYKUL, H. (2017).

Static behavior of lattice structures produced via direct metal laser sintering technology. *Materials & Design*, Vol. 135, pp. 246-256. https://doi.org/10.1016/j.matdes.2017.09.003

[18] PIŠ, D., POUZAROVÁ, H., HANUŠOVÁ, K. (2022). Degradation of 3D Printed Polymer Composites with Filler of Cellulose-Based Materials. *Manufacturing Technology*, Vol. 22, No. 3, pp. 327-333. https://doi.org/10.21062/mft.2022.041

[19] WAFIUDDIN SUHAMI, M., AB WAHAB, N., BOEJANG, H., HAMZAH, K., SASAHARA, H. (2022). Characteristics of Pinewood Dust Combined with Vinyl Ester Composites Through Material Testing and Machining. *Manufacturing Technology*, Vol. 22, No. 5, pp. 590-597. https://doi.org/10.21062/mft.2022.063

[20] CAO, X., JIANG, Y., ZHAO, T., WANG, P., WANG, Y., CHEN, Z., FANG, D. (2020). Compression experiment and numerical evaluation on mechanical responses of the lattice structures with stochastic geometric defects originated from additive-manufacturing. *Composites Part B: Engineering*, Vol. 194, pp. 108030. https://doi.org/10.1016/j.compositesb.2020.108030

[21] HAWRELIAK, J. A., LIND, J., MADDOX, B., BARHAM, M., MESSNER, M., BARTON, N., KUMAR, M. (2016). Dynamic Behavior of Engineered Lattice Materials. *Scientific Reports*, Vol. 6, pp. 28094. https://doi.org/10.1038/srep28094

[22] YANG, L., YAN, C., CAO, W., LIU, Z., SONG, B., WEN, S., YANG, S. (2019). Compression–compression fatigue behaviour of gyroid-type triply periodic minimal surface porous structures fabricated by selective laser melting. *ActaMaterialia*, Vol. 181, pp. 49-66. https://doi.org/10.1016/j.actamat.2019.09.042

[23] ALOMAR, Z., & CONCLI, F. (2020). A Review of the Selective Laser Melting Lattice Structures and Their Numerical Models. *Advanced Engineering Materials*, Vol. 22, No. 12, pp. 2000611. https://doi.org/10.1002/adem.202000611